Journal of *Marine Science and Engineering*

MDPI

Article

A Methodology to Assess the Sloshing Effect of Fluid Storage Tanks on the Global Response of FLNG Vessels

Diego F. Hernández-Ménez [1,2], Iván Félix-González [3], José Hernández-Hernández [2,*] and Agustín L. Herrera-May [1,4,*]

[1] Facultad de Ingeniería de la Construcción y el Hábitat, Universidad Veracruzana, Boca del Rio 94294, Mexico
[2] Facultad de Ingeniería Mecánica y Ciencias Navales, Universidad Veracruzana, Boca del Rio 94294, Mexico
[3] Exploration and Production Technologies Center, Mexican Petroleum Institute, Boca del Rio 94286, Mexico; 5ifelix@imp.mx
[4] Micro and Nanotechnology Research Center, Universidad Veracruzana, Boca del Rio 94294, Mexico
* Correspondence: josehernandez02@uv.mx (J.H.-H.); leherrera@uv.mx (A.L.H.-M.); Tel.: +52-229-775-2000 (A.L.H.-M.)

Abstract: The sloshing effect of fluid storage tanks of a Floating Liquefied Natural Gas (FLNG) vessel causes variations in its global motion response. These acceleration and motion alterations can affect the safe performance of the FLNG vessels. The classification societies' rules are employed to standardize the storage tanks' configuration of FLNG vessels. Herein, we report a methodology to assess the sloshing effect on the global motion response of an FLNG vessel considering four geometrical arrangements of tanks and different fluid filling fractions. This methodology includes the hydrodynamic effect in operating and storm conditions from the Gulf of Mexico using a return period of 100 years. In addition, our methodology considers the influence of the internal fluid of each tank to estimate the accelerations and motions of the vessel. This methodology can be implemented to estimate the stability of an FLNG vessel under different environmental conditions. Thereby, the naval engineers could choose the best geometrical configuration of the storage tanks for safe behavior of a vessel under different operating and extreme environmental conditions.

Keywords: sloshing effect; FLNG; hydrodynamic analysis; vessel; fluid storage tank

Citation: Hernández-Ménez, D.F.; Félix-González, I.; Hernández-Hernández, J.; Herrera-May, A.L. A Methodology to Assess the Sloshing Effect of Fluid Storage Tanks on the Global Response of FLNG Vessels. *J. Mar. Sci. Eng.* **2023**, *11*, 1435. https://doi.org/10.3390/jmse11071435

Academic Editors: Bin Xu, Yanmei Jiao and Xi Shen

Received: 24 May 2023
Revised: 15 July 2023
Accepted: 16 July 2023
Published: 18 July 2023

1. Introduction

Floating Liquefied Natural Gas (FLNG) vessels can operate in remote ocean areas transporting liquefied natural gas, which during the LNG upload process are presented with different filling fractions in tanks. Sloshing occurs in transport operations, when liquid movement occurs inside tanks; the impact probably happens on tank walls, with damage. Hu et al. [1] reported that LNG-tank sloshing has an important contribution to roll motion while its influence on the other motion modes is relatively negligible on an FLNG vessel. In addition, they indicated that the inner tank sloshing has a significant influence on the roll motion of the FLNG vessel. The impact of inner tank sloshing on roll motion is related to the wave-approaching angle and inner-tank filling fraction. Generally, the sloshing motion of this fluid is only considered in the initial design of a vessel. However, this sloshing phenomenon should also be studied if the vessel is modified to move other fluid cargo types. For the design and operation of an FLNG vessel, the naval designers must investigate the sloshing effect of the internal fluid in the tanks on the global motion response and the vessel's structural behavior in order to ensure the safe performance of the vessel under different operating and extreme environmental conditions [2–5].

In conventional ship-motion analysis, the effects of inner free surfaces and sloshing inside the tanks are usually ignored; however, recent experimental and numerical studies have shown that the effects, between a fluid cargo and the LNG ship motion, can be significant at certain filling levels [6–8]. The coupling effect between the vessel motion and

sloshing in tanks generates forces and moments that can cause large deformations and stresses on the internal structure of tanks [9,10]. The sloshing flow can be increased when the external wave frequency agrees with that of the vessel motion coupled with cargo in the tanks. Moreover, vessel stability with partially filled tanks depends on both external wave motion and internal flow [11–13]. Thus, the study of this coupling effect is very important to obtain the reliable structural design of the tanks and maintain the stability of vessels.

Zhuang and Wan [13] described the coupling effects between the motion of a Floating, Production, Storage, and Offloading (FPSO) and sloshing in LNG tanks using Computational Fluid Dynamics (CFD) simulations. They studied this coupling effect between the impact of different wave amplitudes and frequencies and liquid filling conditions. DNV-GL described a methodology to evaluate the structural behavior of tanks containing natural gas and the loads generated by the sloshing motion [14,15]. In addition, the Bureau Veritas Society [16] reported a guidance note to calculate the design sloshing loads in a cargo membrane tank that contains liquefied natural gas (LNG). This guidance note is applied to offshore LNG floating units employing membrane tanks, obtaining the sloshing loads on the cargo tanks and on the inner hull structure. Dioni [17] studied the sloshing effect in the hydrodynamic interaction between two vessels using numerical simulations. Dumitrache and Deleanu [18] registered the fluid–structure interaction of ballast tanks using numerical simulations with the transient module. These simulations determined the pressure on the structure of the tanks due to the sloshing motion of two fluids (seawater and air) inside the tanks. Furthermore, the distributions of the deformation and von Mises stress on the structure of the tanks were obtained. Liu [19] developed a nonlinear coupled numerical model to predict the liquid sloshing in LNG tanks affected by ship motions. This model included the coupling effects between nonlinear–viscous sloshing flows and nonlinear ship motions. Krata and Wawrzyński [20] studied the rolling amplitude of a ship considering the liquid sloshing in partly filled tanks using CFD simulations. This investigation estimated the typical and extreme rolling values of a vessel. He et al. [21] studied the response of a ship with and without a tank using CFD models and experimental results. They investigated dissimilar working conditions and the influence of the liquid height in the tank, tank size, and the wavelength ratio of the incident wave on the vessel motion. Kawahashi et al. [22] performed tests to investigate the coupling effect of FLNG motions with internal sloshing flow. This test included an FLNG model equipped with six square tanks under a fixed solid-cargo condition and a liquid-cargo condition. They observed nonlinear free surface motion for the case of low filling level in tanks. Lyu et al. [23] described a computational procedure to estimate the free surface flow in tanks and the ship motion in regular head and beam waves.

Herein, we propose a methodology to predict the sloshing effect on the global motion response of an FLNG vessel considering four geometrical arrangements of tanks with different fluid filling fractions. This sloshing motion is obtained based on the hydrodynamic influence for both operating and storm cases from the Gulf of Mexico using a return period of 10 years to operative conditions (calm sea) and 100 years to hurricane conditions (storm). Furthermore, the proposed methodology considers the effect of the dynamic of the internal fluid of the tank to determine the acceleration and motion of the FLNG vessel. This methodology can be used to study the stability of vessels coupled with partially filling tanks under different hydrodynamic conditions. Our methodology can be used for the analysis of the behavior of stored fluid with six degrees of freedom, focusing on motions and accelerations due to sloshing effects.

2. Method

The proposed methodology was applied to an FLNG vessel considering four different geometric arrangements of storage tanks and variable filling fractions. This methodology included the following three stages (see Figure 1):

- Stage 1: Four 3D hull models of an FLNG vessel with different geometric arrangements of storage tanks are built through SeSam GeniE DNV software. These models incorporated the distribution of compartments in the hull.
- Stage 2: Based on HydroD SeSam DNV software, the hydrodynamic analysis for the 3D hull models is achieved. For this analysis, the data are processed employing PostResp SeSam DNV. These data are obtained regarding the operational area for the FLNG vessel. For this case, the data used consider the operating and hurricane environmental contours from the Gulf of Mexico, including a return time of 100 years.
- Stage 3: The maximum responses of each 3D hull model are estimated employing the hydrodynamic data. Later, all data are compared to study the sloshing effect on the global motion response of the FLNG vessel.

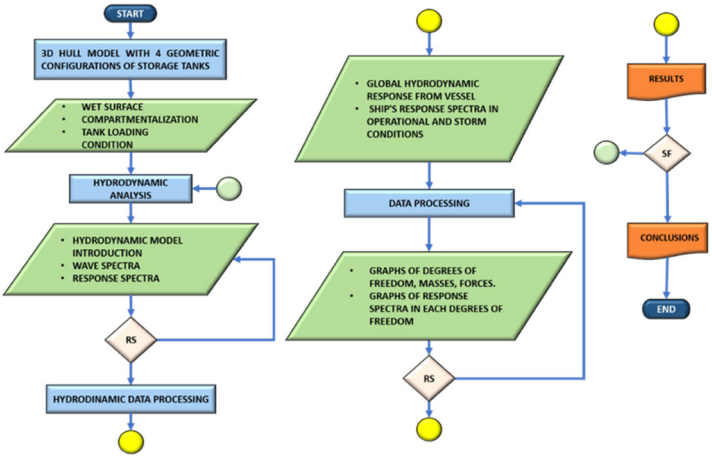

Figure 1. Schematical view of our methodology to estimate the sloshing effect on the global motion response of an FLNG vessel with four geometric arrangements of storage tanks. (RS: Results review and SF: Final results analysis).

2.1. D Hull Models of an FLNG

Table 1 depicts the 3D hull models of an FLNG vessel, which are drawn with SeSam GeniE DNV software. These models regarded the compartments for the natural gas and the ballast tanks of water storage, and a housing module of the FLNG (see Figures 2 and 3). The housing module represents a weight that is added to the FLNG. Figure 4 illustrates the 3D models, which consider the wet surface of the FLNG vessel created with SeSam GeniE DNV software. Figure 5 shows the meshed models of the FLNG vessel, which include the mass related to the housing module. Figures 6–8 show the dimensions for each geometric storage tank. Figure 9 illustrates the dimensions of the FLNG hull model.

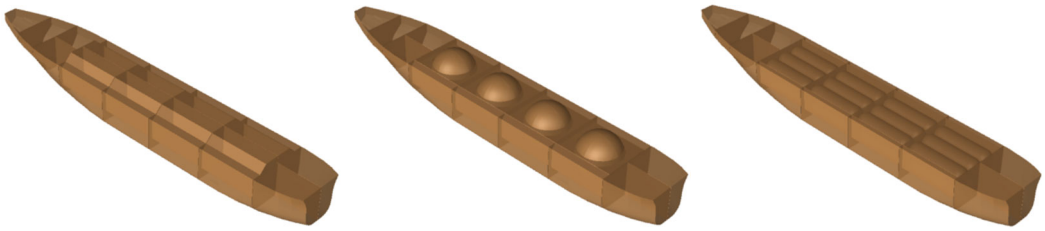

(**a**) (**b**) (**c**)

Figure 2. 3D hull models with compartments of the FLNG vessel with (**a**) prismatic tanks, (**b**) spherical tanks, and (**c**) cylindrical tanks drawn with SeSam GeniE DNV software.

Table 1. 3D hull models and volume capacities of the FLNG vessel developed using SeSam GeniE DNV software.

Model	Tanks Number	Volume by Tank (m^3)	Total Volume (m^3)
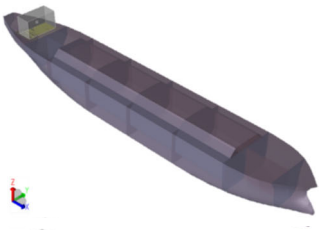	4	33,032	132,128
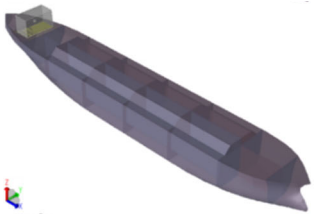	8	16,516	132,128
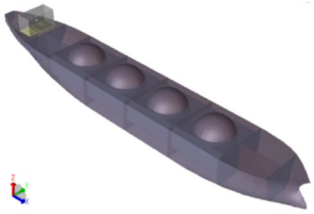	4	13,524	54,096
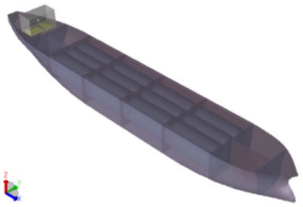	24	2879.8	69,115.2

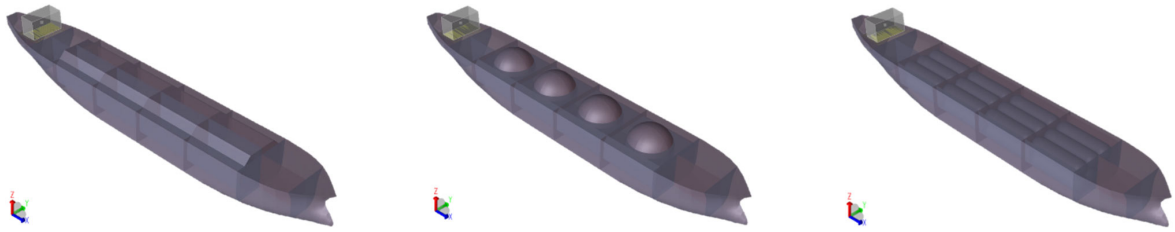

(**a**) (**b**) (**c**)

Figure 3. 3D hull models with housing module of the FLNG vessel with (**a**) prismatic tanks, (**b**) spherical tanks, and (**c**) cylindrical tanks obtained with SeSam GeniE DNV software.

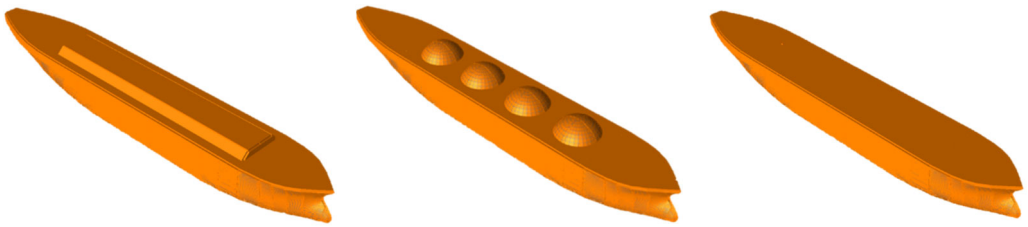

(**a**) (**b**) (**c**)

Figure 4. 3D hull models that regard the wet surface of the FLNG vessel with (**a**) prismatic tanks, (**b**) spherical tanks, and (**c**) cylindrical tanks obtained with SeSam GeniE DNV software.

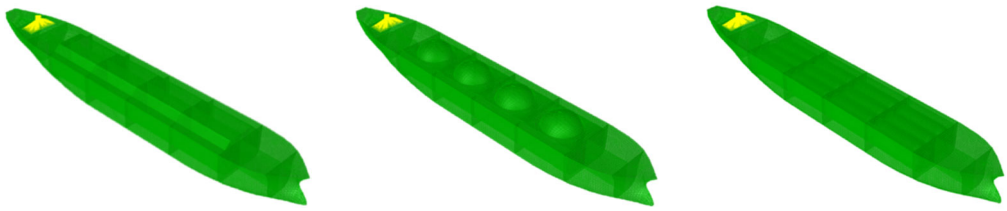

(a) (b) (c)

Figure 5. Meshed 3D hull models of the FLNG vessel with (**a**) prismatic tanks, (**b**) spherical tanks, and (**c**) cylindrical tanks considering the mass of the housing equipment module. These models are developed using SeSam GeniE DNV software (Manager V6.1-02).

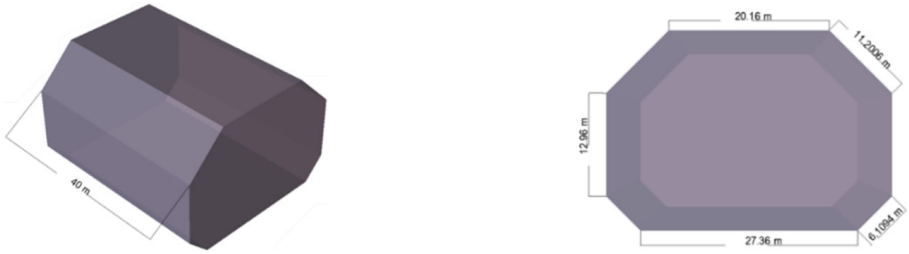

(a) (b)

Figure 6. View of the (**a**) 3D model and (**b**) dimensions of the prismatic storage tank of the FLNG vessel drawn with SeSam GeniE software (manager V6.1-02).

(a) (b)

Figure 7. View of the (**a**) 3D model and (**b**) dimensions of the divided prismatic storage tank of the FLNG vessel drawn using SeSam GeniE software (manager V6.1-02).

(a) (b)

Figure 8. Dimensions of (**a**) spherical storage tank and (**b**) cylindrical storage tank of the FLNG vessel obtained using SeSam GeniE software (manager V6.1-02).

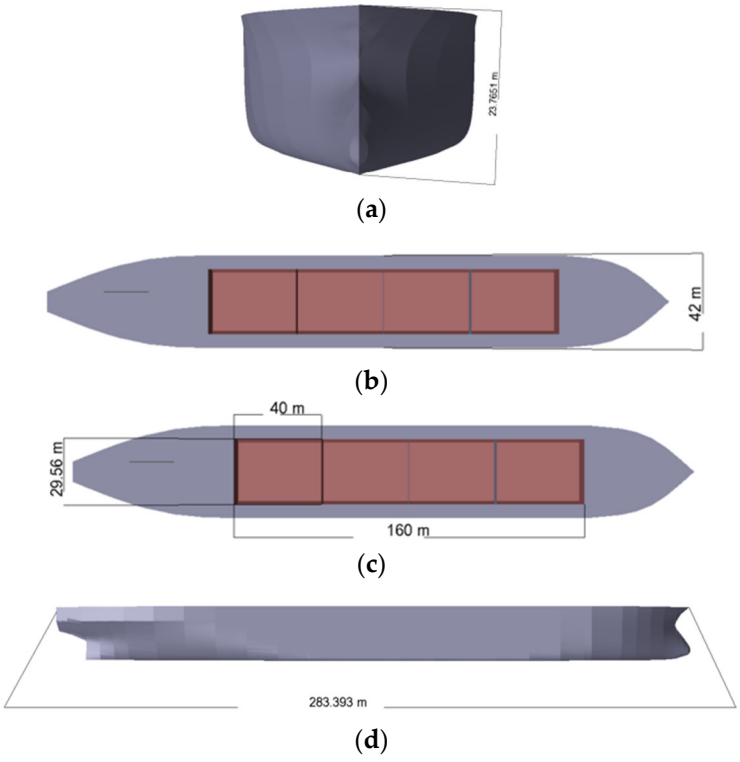

Figure 9. 3D hull model of the FLNG: (**a**) depth, (**b**) breadth, (**c**) storage tank area, and (**d**) length.

The panel model is employed to determine the hydrodynamic loads and responses using the potential theory. The panel model includes panels representing the wet ship surfaces. In the paper, the panel is modeled in SeSam GeniE DNV using a standard size of finite elements of 1.6 m. The panel is constructed using segments of straight lines between corner nodes of the sides of finite elements. For a panel, the wet surface is obtained through a dummy load on the panel model in SeSam GeniE DNV, regarding a load case number of 1 to all external wet surfaces of the model [24].

2.2. Hydrodynamic Analysis

The velocity potential theory is applied to determine the effects of first-order radiation and diffraction on large-volume structures using the 3D panel method to assess the velocity potentials and hydrodynamic coefficients. The free surface conditions are linearized using the first-order potential theory. The radiation and diffraction velocity potentials on the wet surface of the structure are estimated from the solution for the integral equation obtained by Green's theorem by considering free surface potentials as Green's functions. Boundary value problems are solved with Green's theorem to obtain integral equations for the radiation and diffraction velocity potentials on body boundaries. The integral Equation (1) considers the radiation velocity potentials f_j on the body boundary [25]:

$$2\pi\phi_j(x) + \iint_{Sb} \phi_j(\xi)\frac{\partial G(\xi;x)}{\partial \eta_\xi}d\xi = \iint_{Sb} \eta_j G(\xi;x)d\xi \quad (1)$$

where S_b is the mean wet surface of the body and η is the unit vector. Green's function $G(\xi;x)$ is the velocity potential at field point x caused by a point source located at point ξ. Total diffraction velocity potential ϕ_D is shown in Equation (2) [25]:

$$2\pi\phi_D(x) + \iint_{Sb} \phi_D(\xi)\frac{\partial G(\xi;x)}{\partial \eta_\xi}d\xi = 4\pi\phi_0(x) \quad (2)$$

The components of one-time fluid velocity are determined, and the integral equation is transformed in the following general form for source instead of velocity potential (see Equation (3)), [25].

$$2\pi\sigma(x) + \iint_{Sb} \sigma(\xi)\frac{\partial G(\xi;x)}{\partial \eta_x}d\xi = \frac{\partial \phi(x)}{\partial \eta_x} \quad (3)$$

For 3D hull models of the FLNG vessel, their hydrodynamic analyses are described with the following issues:

- The hydrodynamic analysis considers the following two cases: with and without the dynamic effect of internal fluid. In this analysis, the variation of the vessel performance using both cases with and without the sloshing motion is compared.
- Twenty-four orientations of wave directions are studied to describe the location of the vessel to the plane in increments of 15° from 0 to 360°.
- Eight filling fractions in the tank are studied to obtain the behavior of the sloshing effect, which ranges from 10 to 80 percent in increments of 10%.
- For all models, the base draught for the FLNG vessel is established at 9.6 m.

These issues are the main conditions to determine the hydrodynamic analysis of the FLNG vessel. Furthermore, the wave periods that generate the most significant energy are selected. The maximum magnitude of the period is established at 35 s. The wave period begins in 3 s because at this time the energy begins to be important. Figure 10 shows a wave-scattering diagram that describes the estimated environmental contour for the sea area of the Gulf of Mexico. In this paper, the data used is for 100-year prediction. Table 2 shows the parameters of the environmental fluids and gravity employed in our hydrodynamic analysis. The characteristics of the hydrodynamical model are indicated in Table 3. Wave analysis by diffraction and Morrison Theory (Wadam), used by HydroD SeSam DNV in hydrodynamic analysis, used a global response analysis for a ship with no forward speed [25].

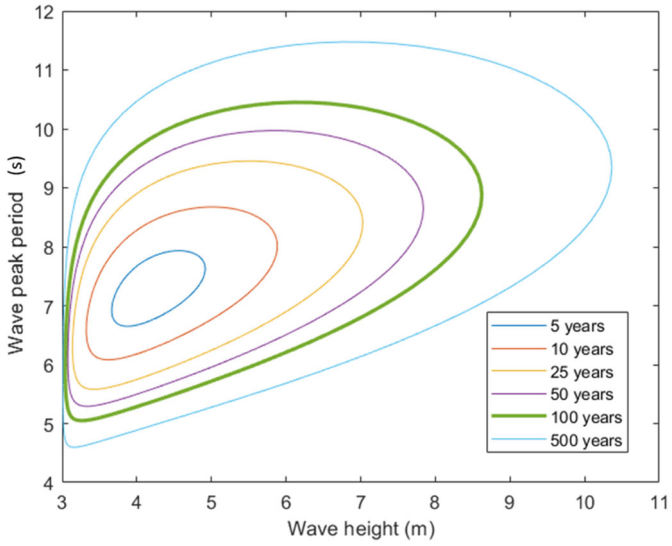

Figure 10. Environmental contours used for the sea area of the Gulf of Mexico.

Table 2. Parameters of the fluids and gravity employed in the hydrodynamic analysis of the FLNG vessel.

Parameter	Density (kg/m^3)	Kinematic Viscosity (m^2/s)	Depth (m)	Value (m/s^2)
Gravity	-	-	-	9.80665
Air	1.266	1.462×10^{-5}	-	-
Water	1025	1.19×10^{-6}	1000	-

Table 3. Characteristics of the hydrodynamical model of the FLNG vessel.

Position	Value (m)
Baseline z	0
AP x	−6
FP x	280

Table 4 depicts the number of panels for each model. The basic part of the panel is modeled as one first-level superelement. The coordinate system for the model is located at the water level above the center of gravity [25]. In each load case, the filling level by the tank is determined to employ the ideal equilibrium state for each filling fraction. Table 5 shows the density of the cargo fluids used in the hydrodynamic analysis.

Table 4. Number of panels of each model and the geometric configuration of the tank.

Permeability	Number of Generated-Basic Panels			
	Prismatic	Divided Prismatic	Spherical	Cylindrical
10%	3096	3096	4703	4942
20%	3258	3258	4922	5120
30%	3441	3441	5080	5330
40%	3632	3632	5303	5503
50%	4084	4084	5437	5702
60%	4084	4084	5949	5876
70%	4084	4084	5754	6248
80%	4084	4084	5935	6248

Table 5. Values of the densities of the cargo fluids stored in the FLNG storage tanks.

Fluid	Density (kg/m^3)
Liquid natural gas (LNG)	450
Sea water	1025

In each load case, the equilibrium condition of the FLNG vessel is affected by the filling level for each tank. For this condition, the tanks are individually built. Next, the hydrodynamic analysis of the FLNG vessel evaluates the off-body points (see Table 6) that establish the representative location for the sea level. Figure 11 illustrates the 3D hydrodynamical model in the equilibrium state of an FLNG vessel, which is developed employing the SeSam HydroD DNV software. Equation (4) shows the viscous damping matrix used for the hydrodynamic analysis, which considers its effect on the response of all freedom degrees [3].

$$\beta = \begin{bmatrix} 0.05 & 0 & 0 & 0 & 0 & 0 \\ 0 & 0.05 & 0 & 0 & 0 & 0 \\ 0 & 0 & 0.05 & 0 & 0 & 0 \\ 0 & 0 & 0 & 0.05 & 0 & 0 \\ 0 & 0 & 0 & 0 & 0.05 & 0 \\ 0 & 0 & 0 & 0 & 0 & 0.05 \end{bmatrix} \quad (4)$$

Table 6. Offbody point definition for hydrodynamic analysis of an FLNG vessel.

Item	Value (m)
Max point x	392
Max point y	38
Min point x	−119
Min point y	−38

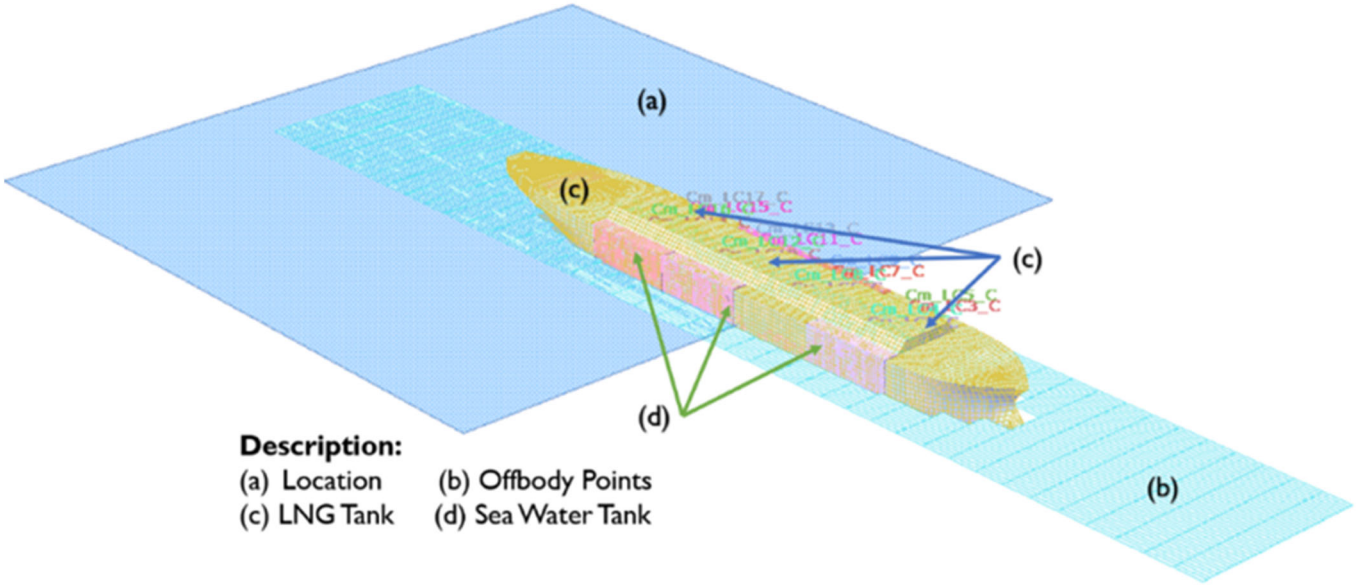

Figure 11. View of the 3D hull model of an FLNG vessel. This model regards the sea position for its hydrodynamic analysis, which is evaluated through the SeSam HydroD software.

2.3. Data Analysis

Figure 12 depicts the stages of the algorithms used in the data processing of the hydrodynamic analysis of an FLNG vessel, which is implemented in MATLAB 2017b software.

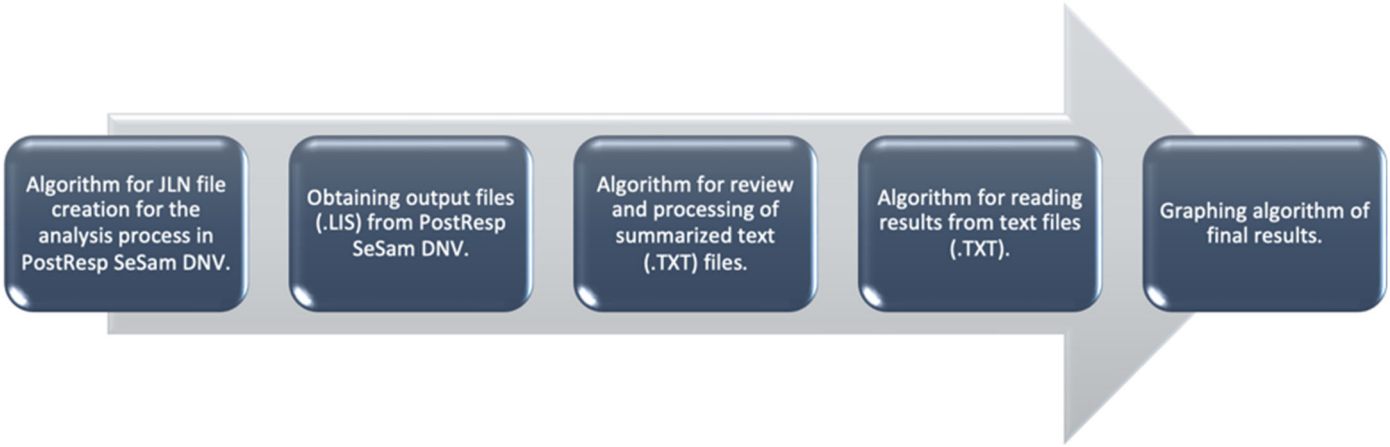

Figure 12. Data processing of the hydrodynamic analysis of a FLNG vessel.

The Response Amplitude Operators (RAOs) assess the performance of the vessel in its six degrees of freedom for a unit wave value and the global motion response of the vessel including the sloshing effect. These RAOs can be determined using Equation (5):

$$M\ddot{x} + B\dot{x} + Kx = f(t) \quad (5)$$

where M is the mass, B is the damping and K is the hydrostatic stiffness coefficient of the ship, and $f(t)$ is the function of external environmental force.

By using the frequency domain with $\omega^2 = K/M$, the following constant C is used to predict the RAOs [2]:

$$C = \frac{F}{K} \frac{1}{\left[1 - \frac{\omega_R{}^2}{\omega^2} + \frac{\beta i \omega}{K}\right]} \tag{6}$$

where F is the magnitude of force, ω_R is the excitation angular frequency, ω is the natural angular frequency, β is the damping factor, and i the imaginary unit.

The Pierson-Moskowitz (PM) wave spectra (S_{PM^ω}) are studied by using the environmental contours of the location [2] with a return time of 100 years, which describes the sea state conditions at the specific location (hypothetically).

$$S_{PM^\omega} = \frac{5}{16} {H_S}^2 {\omega_p}^4 \omega^{-5} \exp\left[-\frac{5}{4}\left(\frac{\omega}{\omega_p}\right)^{-4}\right] \tag{7}$$

where ω_p is the spectral peak angular frequency and H_s is the wave height. Then, the model response spectra (S_R) are determined by Equation (8).

$$S_R = C^2 S_{PM^\omega} \tag{8}$$

With these spectra, the most probable maximum responses are calculated.

3. Results and Discussion

3.1. Dynamic of Internal Fluid

The hydrodynamic analysis of the FLNG vessel with four geometric configurations of storage tanks includes the sloshing effect using the Wadam Wizard with a panel model in the frequency domain considering Pierson–Moskowitz wave spectra. The most probable maximum responses are compared including (or not) the dynamics of internal fluid, storm (hurricane) case, and regular operating (calm sea) conditions. Figure 13 depicts the comparative graphs of the most probable maximum responses of the sloshing effect between acceleration and fluid motion in the six degrees of freedom. The maximum responses regarding the sloshing effect under acceleration under regular operating and storm conditions are 71% and 69%, respectively. In addition, the maximum results of sloshing effects in motion under regular operating and storm conditions are 62% and 58%, respectively. Tables 7 and 8 indicate the filling fractions of the highest most probable maximum responses between cases that consider the dynamic internal fluid for both regular operating and storm conditions under acceleration and in movement, respectively.

Table 7. Comparison of the highest probable maximum acceleration responses between cases with and without considering the effect of the internal fluid dynamics for the regular operating and storm cases of the four geometric arrangements of the storage tanks. The numbers represent eight analyses.

Freedom Degree	Acceleration															
	Prismatic Tank				Divided Prismatic Tank				Spherical Tank				Cylindrical Tank			
	OP		H		OP		H		OP		H		OP		H	
	D	ND	D	ND	D	ND	D	ND	D	ND	D	ND	D	ND	D	ND
Heave	5	1	5	1	6	1	6	1	5	3	5	3	5	1	5	1
Surge	8	0	8	0	7	0	8	0	8	0	8	0	7	0	7	0
Sway	7	1	5	1	7	1	7	1	5	3	5	3	6	1	6	1
Yaw	4	4	3	5	6	2	6	2	4	4	4	4	7	1	6	2
Roll	3	5	2	6	7	1	7	1	4	3	4	3	6	1	6	1
Pitch	2	6	2	6	4	4	3	5	2	6	2	6	4	3	5	2

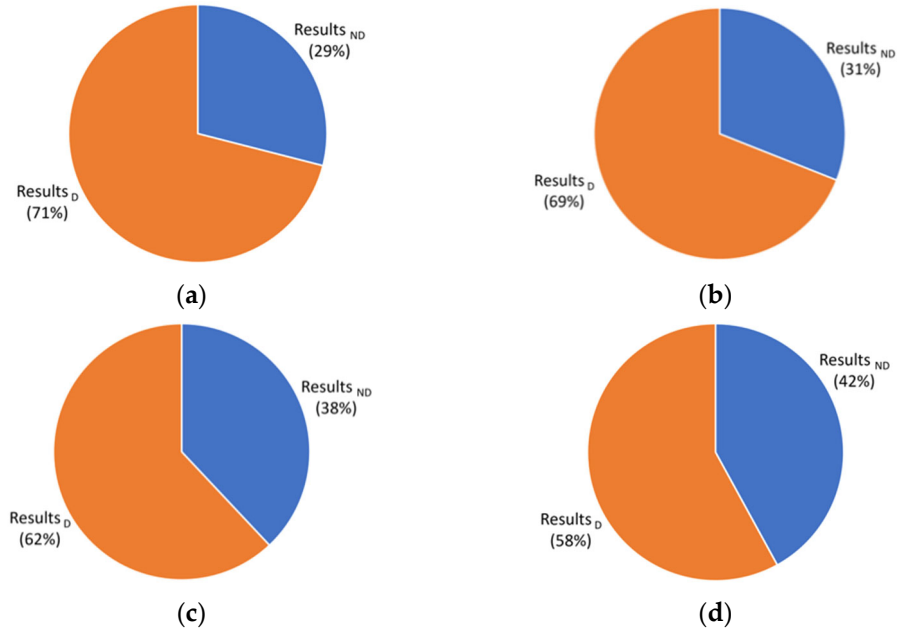

Figure 13. Comparative graphs of the most probable maximum responses of the sloshing effect for the six degrees of freedom: (**a**) Acceleration under regular operating conditions (calm sea), (**b**) acceleration under storm conditions (hurricane), (**c**) motion under regular operating conditions (calm sea), and (**d**) motion under storm conditions (hurricane). Note: D and ND represent the dynamic and non-dynamic internal fluid conditions.

Table 8. Comparison of the highest probable maximum motion responses between cases with and without considering the effect of the internal fluid dynamics for the regular operating and storm cases of the four geometric arrangements of the storage tanks. The numbers represent eight analyses.

Freedom Degree	Motion															
	Prismatic Tank				Divided Prismatic Tank				Spherical Tank				Cylindrical Tank			
	OP		H		OP		H		OP		H		OP		H	
	D	ND	D	ND	D	ND	D	ND	D	ND	D	ND	D	ND	D	ND
Heave	2	4	1	5	7	1	6	2	4	3	4	3	6	1	6	1
Surge	8	0	8	0	8	0	8	0	8	0	8	0	8	0	8	0
Sway	1	7	0	8	5	3	5	3	4	4	4	4	5	2	5	2
Yaw	1	7	0	8	6	2	6	2	4	4	4	4	6	2	6	2
Roll	1	7	1	7	7	1	6	2	4	3	4	3	7	1	6	2
Pitch	1	7	0	8	4	4	4	4	3	5	2	6	5	2	5	2

In the acceleration case, the highest response spectra prevail when considering the dynamics of internal tank fluid, but prismatic and spherical tanks have a greater tolerance in rotational freedom degrees. This quality is altered by reducing the containment space in cylindrical and divided prismatic tanks. In the case of freedom degrees, translational ones are more affected by internal fluid dynamics than rotational ones.

In the motion case, the influence of internal fluid dynamics is a condition for the amplitude of contained space. The prismatic and spherical tanks show more tolerance under both operating conditions, but cylindrical and divided prismatic tanks depict the highest response spectra when the internal fluid dynamic is considered.

In both cases, motions and accelerations, the trend shows the most reliability in the cases considering the dynamics of internal fluid in tanks for all the geometries analyzed, since there are few cases where the highest value of analysis does not contemplate the internal dynamic of fluid stored in tanks.

3.2. Sloshing Effect in Heave

Tables 9 and 10 show a summary of the most probable maximum acceleration and motion responses of the sloshing effect considering four tank geometries on an FLNG vessel, respectively. The number 0 represents a negligible response between considering (or not) the internal fluid dynamics. The number 1 indicates the highest response between considering (or not) the internal fluid dynamics. Figures 14 and 15 depict the graphs of the maximum sloshing effect in the heave for the regular operation (calm sea) and storm (hurricane) cases, respectively. For the geometric arrangements of storage tanks, the highest sloshing effect in heave is obtained using the divided prismatic tank in regular operating and storm conditions with accelerations of 1.569 m/s^2 and 2.096 m/s^2, respectively, as well as motions of 3.624 m and 5.994 m for regular operative and storm conditions, respectively.

Table 9. Acceleration results of hydrodynamic analysis of sloshing effect in the heave of an FLNG vessel. Note: The number 0 represents a negligible response between considering (or not) the internal fluid dynamics. The number 1 indicates the highest response between considering (or not) the internal fluid dynamics.

Acceleration																
Filling Fraction	Prismatic Tank				Divided Prismatic Tank				Spherical Tank				Cylindrical Tank			
	OP		H		OP		H		OP		H		OP		H	
	D	ND	D	ND	D	ND	D	ND	D	ND	D	ND	D	ND	D	ND
10%	0	1	0	1	1	0	1	0	1	0	1	0	0	0	0	0
20%	1	0	1	0	1	0	1	0	1	0	1	0	1	0	1	0
30%	1	0	1	0	1	0	1	0	1	0	1	0	1	0	1	0
40%	1	0	1	0	1	0	1	0	1	0	1	0	1	0	1	0
50%	1	0	1	0	0	1	0	1	0	1	0	1	1	0	1	0
60%	0	0	0	0	1	0	1	0	0	1	0	1	0	1	0	1
70%	1	0	1	0	1	0	1	0	1	0	1	0	1	0	1	0
80%	0	0	0	0	0	0	0	0	0	1	0	1	0	0	0	0

Table 10. Heave motion results of hydrodynamic analysis of sloshing effect of an FLNG vessel. Note: The number 0 represents a negligible response between considering (or not) the internal fluid dynamics. The number 1 indicates the highest response between considering (or not) the internal fluid dynamics.

Motion																
Filling Fraction	Prismatic Tank				Divided Prismatic Tank				Spherical Tank				Cylindrical Tank			
	OP		H		OP		H		OP		H		OP		H	
	D	ND	D	ND	D	ND	D	ND	D	ND	D	ND	D	ND	D	ND
10%	0	1	0	0	1	0	0	1	0	0	0	0	0	0	0	0
20%	0	0	0	1	1	0	1	0	1	0	1	0	1	0	1	0
30%	0	1	0	1	1	0	1	0	1	0	1	0	1	0	1	0
40%	1	0	0	1	1	0	1	0	1	0	1	0	1	0	1	0
50%	1	0	1	0	0	1	0	1	0	1	0	1	1	0	1	0
60%	0	1	0	1	1	0	1	0	0	1	0	1	0	1	0	1
70%	0	1	0	1	1	0	1	0	1	0	1	0	1	0	1	0
80%	0	0	0	0	1	0	1	0	0	1	0	1	1	0	1	0

3.3. Sloshing Effect in Roll

Tables 11 and 12 indicate a summary of the most probable maximum rolling acceleration and motion responses of the sloshing effect of the four tank geometries on an FLNG vessel, respectively, for each filling fraction. In both tables, the number 0 indicates a negligible response between considering (or not) the internal fluid dynamics. The number 1 represents the highest response between considering (or not) the internal fluid dynamics. Figures 16 and 17 show the response of maximum rolling acceleration and motion considering the sloshing effect for regular operation and storm cases, respectively. For the

geometric arrangements of storage tanks, the highest sloshing effect in roll is achieved with the divided prismatic tank in regular operating and storm conditions with accelerations of 10.07°/s^2 and 15.34°/s^2, respectively, as well as motion of 27.89° and 56.24° for regular operative and storm conditions, respectively.

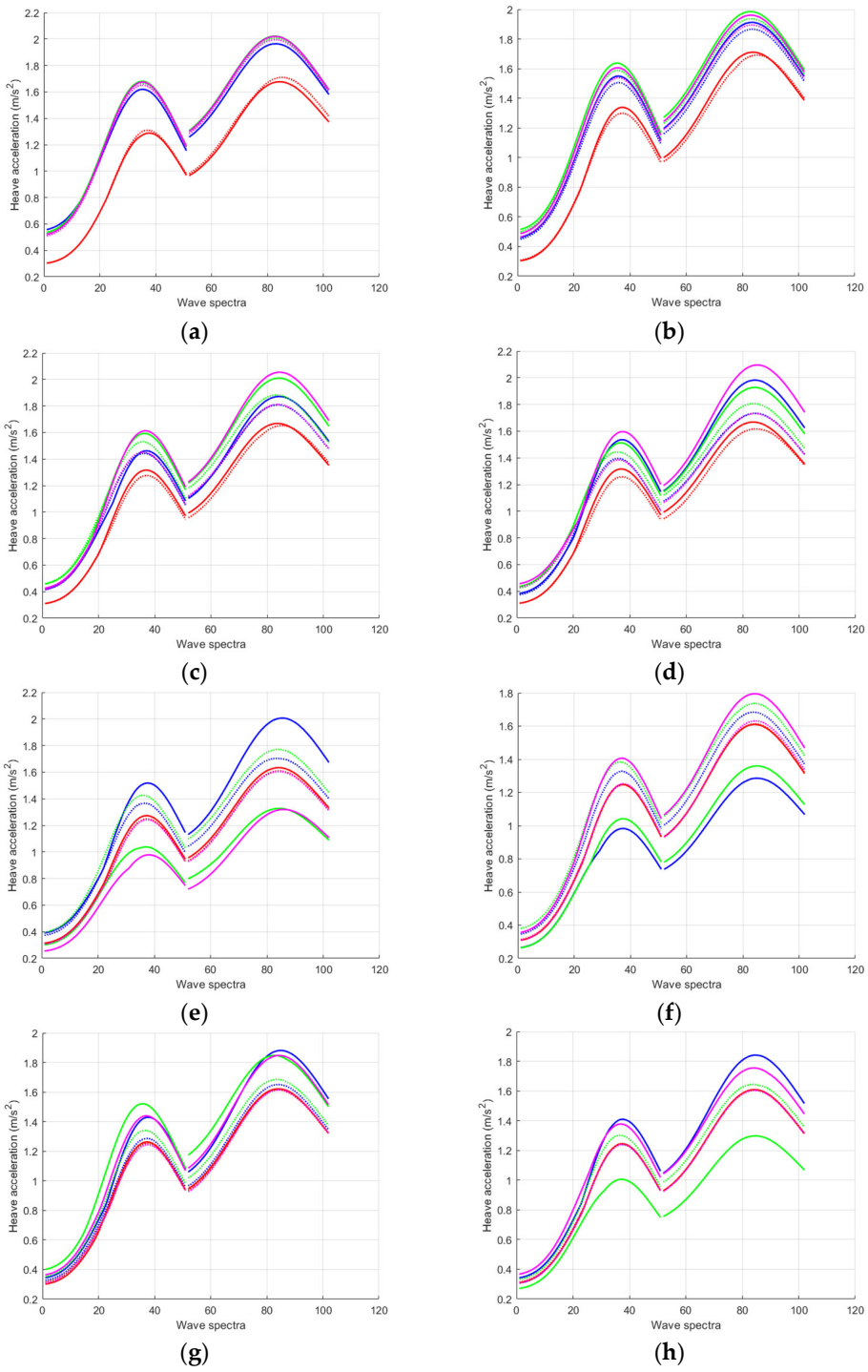

Figure 14. Sloshing effect on the heaving acceleration of FLNG vessel in four tank geometries with filling fraction of (a) 10%, (**b**) 20%, (**c**) 30%, (**d**) 40%, (**e**) 50%, (**f**) 60%, (**g**) 70%, and (**h**) 80%. The lines highlighted with the colors red, pink, green, and blue represent prismatic storage, divided prismatic storage, spherical storage, and cylindrical tanks, respectively. The continuous and dotted lines indicate the dynamic and non-dynamic fluid conditions, respectively.

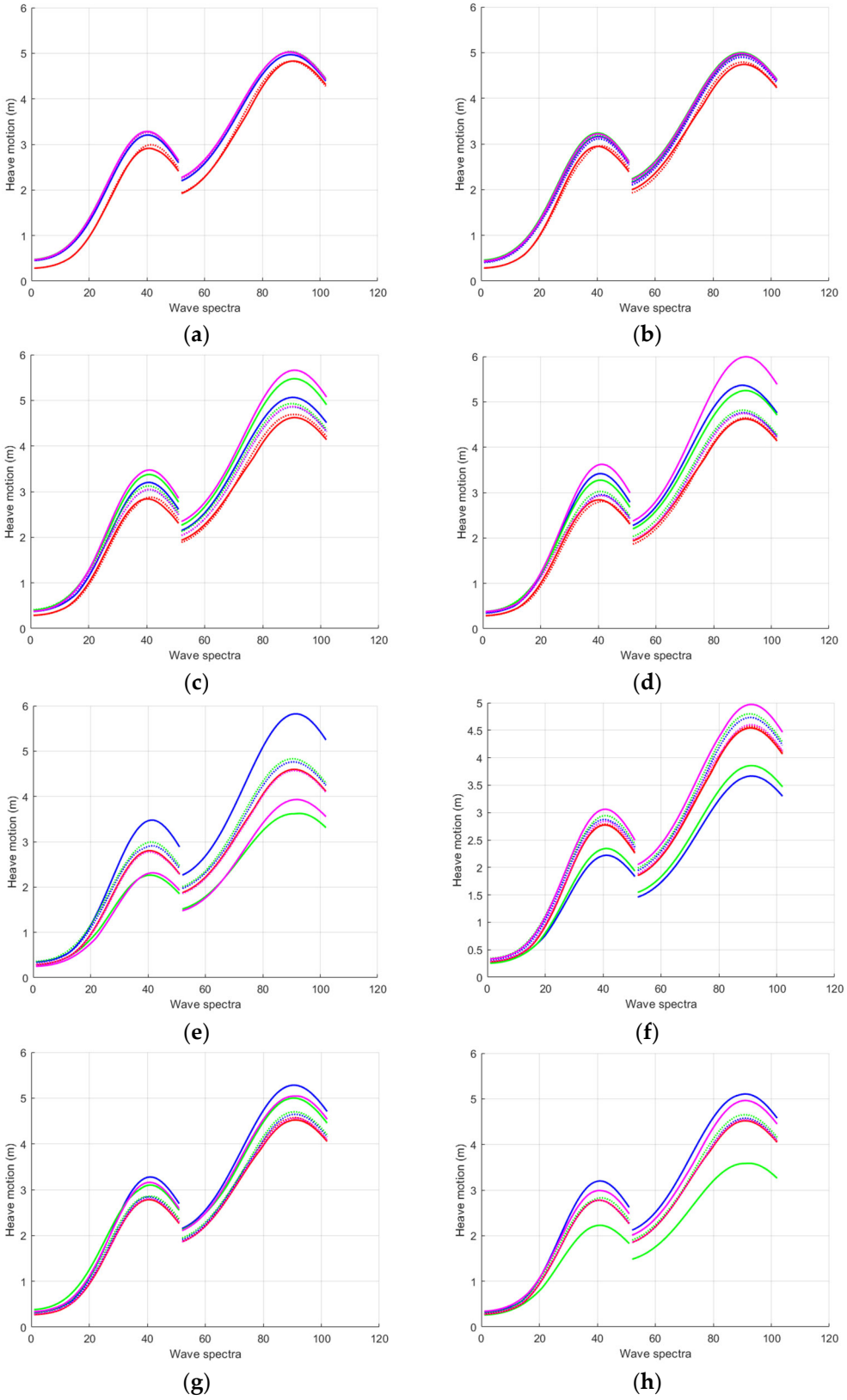

Figure 15. Sloshing effect on the heaving motion of FLNG vessel in four tank geometries with filling fraction of (**a**) 10%, (**b**) 20%, (**c**) 30%, (**d**) 40%, (**e**) 50%, (**f**) 60%, (**g**) 70%, and (**h**) 80%. The lines highlighted with the colors red, pink, green, and blue represent prismatic storage, divided prismatic storage, spherical storage, and cylindrical tanks, respectively. The continuous and dotted lines represent the dynamic and non-dynamic fluid conditions, respectively.

Table 11. Rolling acceleration results of hydrodynamic analysis of sloshing effect of an FLNG vessel. Note: The number 0 represents a negligible response between considering (or not) the internal fluid dynamics. The number 1 indicates the highest response between considering (or not) the internal fluid dynamics.

Rolling Acceleration																
Filling Fraction	Prismatic Tank				Divided Prismatic Tank				Spherical Tank				Cylindrical Tank			
	OP		H		OP		H		OP		H		OP		H	
	D	ND	D	ND	D	ND	D	ND	D	ND	D	ND	D	ND	D	ND
10%	1	0	1	0	1	0	1	0	0	0	0	0	0	0	0	0
20%	1	0	1	0	1	0	1	0	1	0	1	0	1	0	1	0
30%	0	1	0	1	1	0	1	0	1	0	1	0	1	0	1	0
40%	0	1	0	1	1	0	1	0	1	0	1	0	1	0	1	0
50%	1	0	0	1	0	1	0	1	0	1	0	1	1	0	1	0
60%	0	1	0	1	1	0	1	0	0	1	0	1	0	1	0	1
70%	0	1	0	1	1	0	1	0	1	0	1	0	1	0	1	0
80%	0	1	0	1	1	0	1	0	0	1	0	1	1	0	1	0

Table 12. Rolling rotation results of hydrodynamic analysis of sloshing effect of an FLNG vessel. Note: The number 0 represents a negligible response between considering (or not) the internal fluid dynamics. The number 1 indicates the highest response between considering (or not) the internal fluid dynamics.

Rolling Rotation																
Filling Fraction	Prismatic Tank				Divided Prismatic Tank				Spherical Tank				Cylindrical Tank			
	OP		H		OP		H		OP		H		OP		H	
	D	ND	D	ND	D	ND	D	ND	D	ND	D	ND	D	ND	D	ND
10%	0	1	0	1	1	0	0	1	0	0	0	0	1	0	1	0
20%	0	1	0	1	1	0	1	0	1	0	1	0	1	0	1	0
30%	0	1	0	1	1	0	1	0	1	0	1	0	1	0	1	0
40%	0	1	0	1	1	0	1	0	1	0	1	0	1	0	0	1
50%	1	0	1	0	0	1	0	1	0	1	0	1	1	0	1	0
60%	0	1	0	1	1	0	1	0	0	1	0	1	0	1	0	1
70%	0	1	0	1	1	0	1	0	1	0	1	0	1	0	1	0
80%	0	1	0	1	1	0	1	0	0	1	0	1	1	0	1	0

3.4. Sloshing Effect in Pitch

Tables 13 and 14 indicate a summary of the most probable maximum pitch acceleration and motion responses to sloshing effect analysis of the four tank geometries on an FLNG vessel, respectively, at each filling fraction. Figures 18 and 19 illustrate the response of the maximum sloshing effect in pitch for regular operation and storm cases, respectively. For the storage tanks' geometric arrangements, the highest sloshing effect in pitch is obtained using the spherical tank for regular operating and storm conditions with accelerations of $0.601^{\circ}/s^2$ and $0.739^{\circ}/s^2$, respectively, and pitch rotation of 1.239° and 2.028° for regular operative and storm conditions, respectively.

Table 13. Pitch acceleration results of hydrodynamic analysis of sloshing effect of an FLNG vessel. Note: The number 0 represents a negligible response between considering (or not) the internal fluid dynamics. The number 1 indicates the highest response between considering (or not) the internal fluid dynamics.

Pitch Acceleration																
Filling Fraction	Prismatic Tank				Divided Prismatic Tank				Spherical Tank				Cylindrical Tank			
	OP		H		OP		H		OP		H		OP		H	
	D	ND	D	ND	D	ND	D	ND	D	ND	D	ND	D	ND	D	ND
10%	1	0	1	0	0	1	0	1	0	1	0	1	0	0	0	0
20%	1	0	1	0	0	1	0	1	0	1	0	1	0	1	0	1

Table 13. *Cont.*

Pitch Acceleration																
Filling Fraction	**Prismatic Tank**				**Divided Prismatic Tank**				**Spherical Tank**				**Cylindrical Tank**			
	OP		**H**		**OP**		**H**		**OP**		**H**		**OP**		**H**	
	D	**ND**	**D**	**ND**	**D**	**ND**	**D**	**ND**	**D**	**ND**	**D**	**ND**	**D**	**ND**	**D**	**ND**
30%	0	1	0	1	1	0	1	0	1	0	1	0	1	0	1	0
40%	0	1	0	1	0	1	0	1	0	1	0	1	0	1	1	0
50%	0	1	0	1	0	1	0	1	0	1	0	1	1	0	1	0
60%	0	1	0	1	1	0	0	1	0	1	0	1	0	1	0	1
70%	0	1	0	1	1	0	1	0	1	0	1	0	1	0	1	0
80%	0	1	0	1	1	0	1	0	0	1	0	1	1	0	1	0

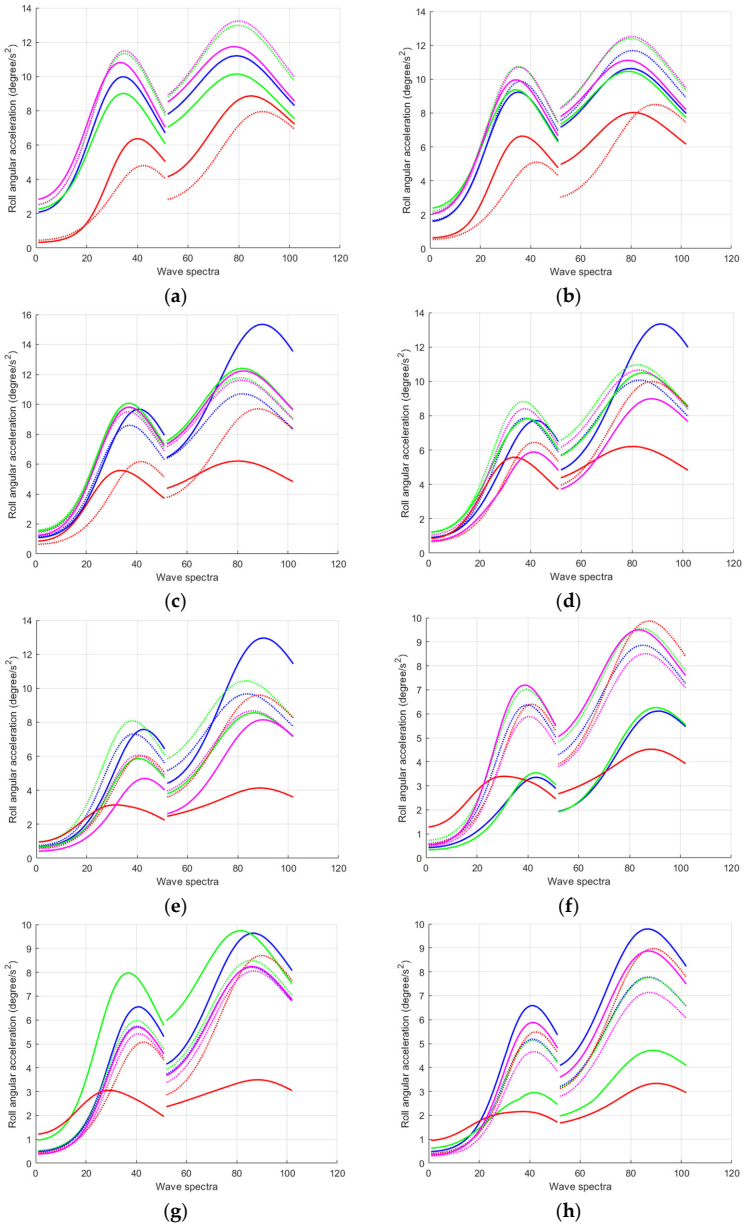

Figure 16. Sloshing effect on rolling acceleration of FLNG vessel for four tank geometries with filling fraction of (**a**) 10%, (**b**) 20%, (**c**) 30%, (**d**) 40%, (**e**) 50%, (**f**) 60%, (**g**) 70%, and (**h**) 80%. The lines highlighted with the colors red, pink, green, and blue represent prismatic storage, divided prismatic storage, spherical storage, and cylindrical tanks, respectively. The continuous and dotted lines represent the dynamic and non-dynamic fluid conditions, respectively.

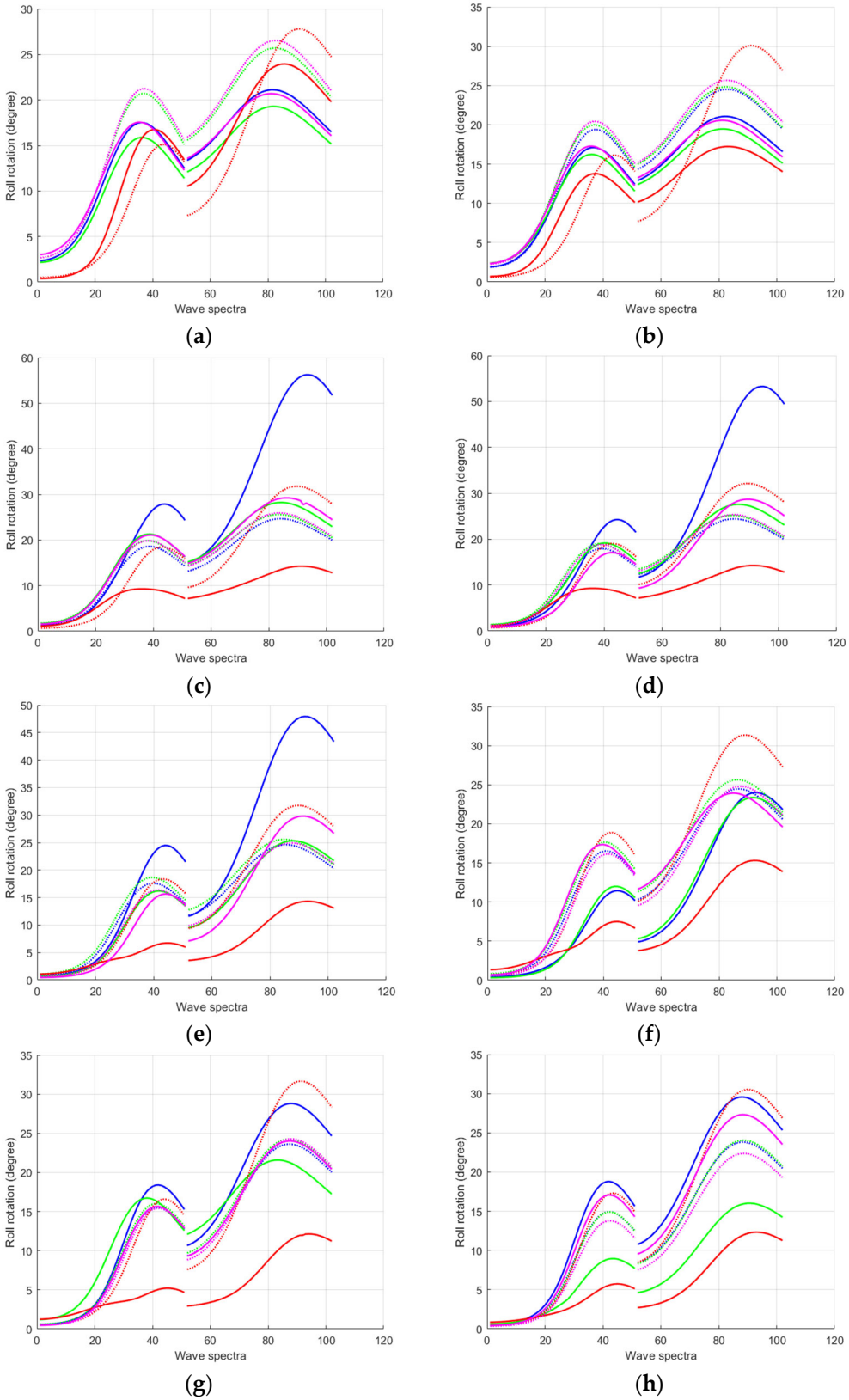

Figure 17. Sloshing effect on rolling motion of FLNG vessel for four tank geometries with filling fraction of (**a**) 10%, (**b**) 20%, (**c**) 30%, (**d**) 40%, (**e**) 50%, (**f**) 60%, (**g**) 70%, and (**h**) 80%. The lines highlighted with the colors red, pink, green, and blue indicate prismatic storage, divided prismatic storage, spherical storage, and cylindrical tanks, respectively. The continuous and dotted lines represent the dynamic and non-dynamic fluid conditions, respectively.

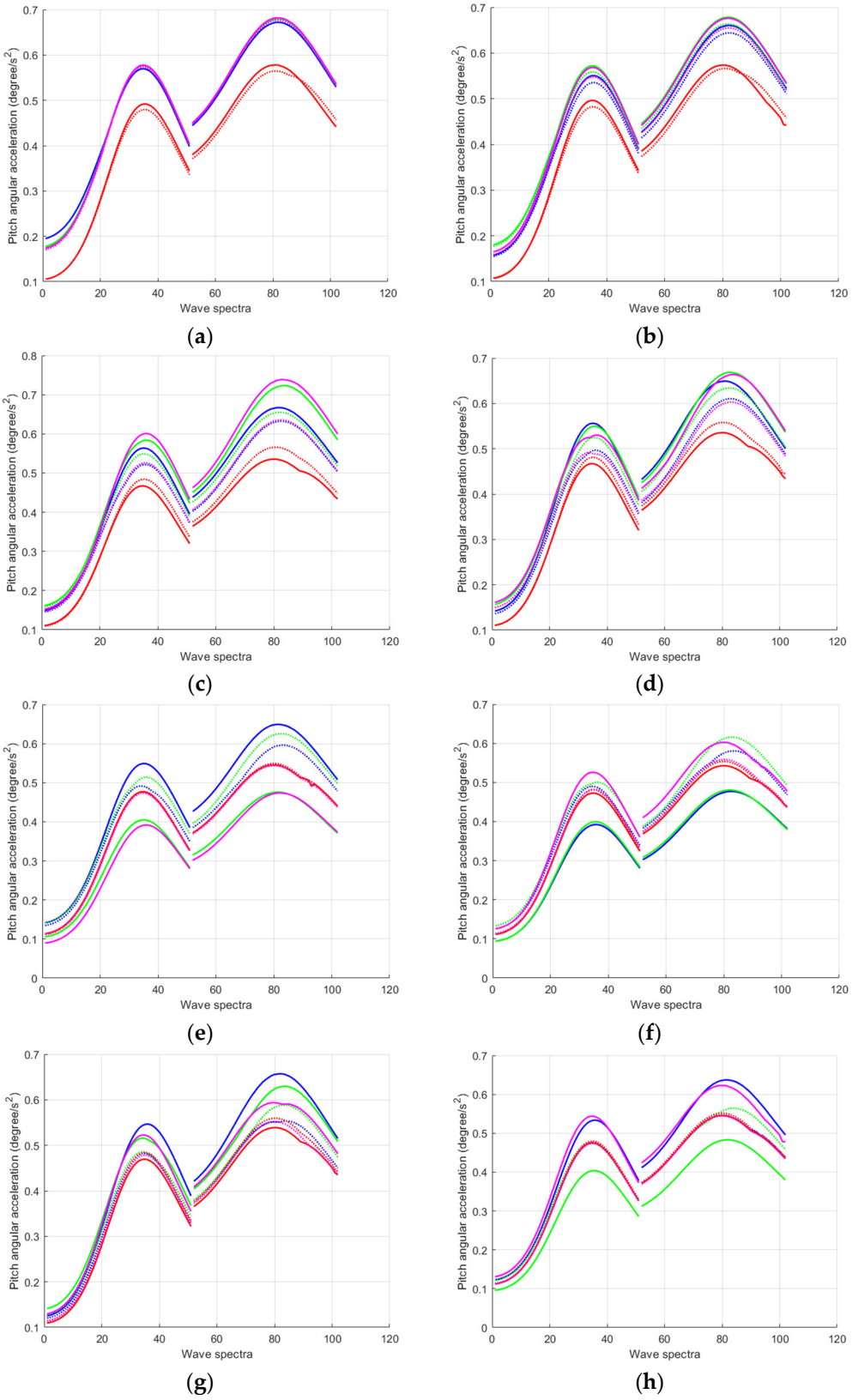

Figure 18. Sloshing effect on pitching acceleration of FLNG vessel for four tank geometries with filling fraction of (**a**) 10%, (**b**) 20%, (**c**) 30%, (**d**) 40%, (**e**) 50%, (**f**) 60%, (**g**) 70%, and (**h**) 80%. The lines highlighted with the colors red, pink, green, and blue indicate prismatic storage, divided prismatic storage, spherical storage, and cylindrical tanks, respectively. The continuous and dotted lines represent the dynamic and non-dynamic fluid conditions, respectively.

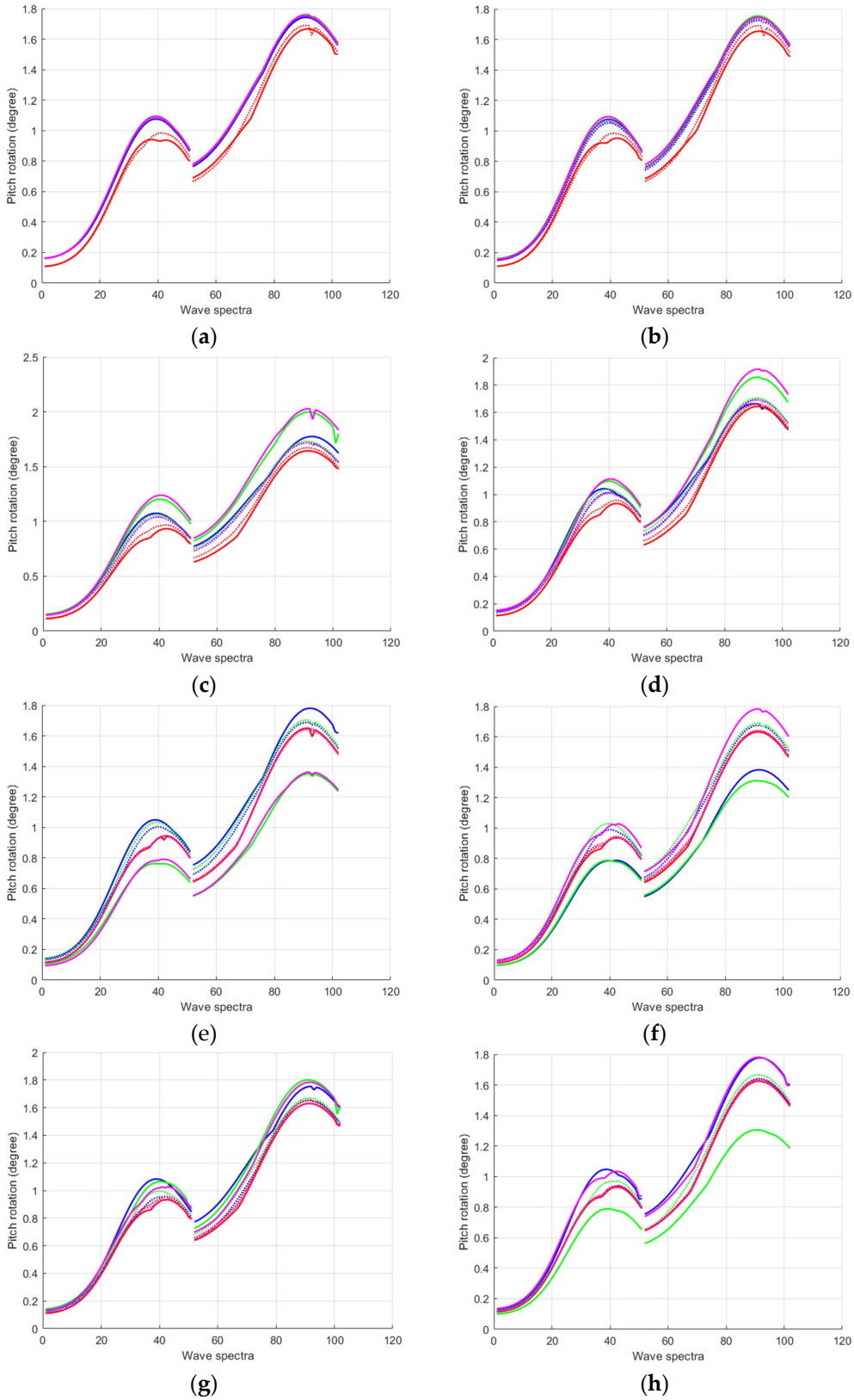

Figure 19. Sloshing effect on pitching motion of FLNG vessel for four tank geometries with filling fraction of (**a**) 10%, (**b**) 20%, (**c**) 30%, (**d**) 40%, (**e**) 50%, (**f**) 60%, (**g**) 70%, and (**h**) 80%. The lines highlighted with the colors red, pink, green, and blue indicate prismatic storage, divided prismatic storage, spherical storage, and cylindrical tanks, respectively. The continuous and dotted lines represent the dynamic and non-dynamic fluid conditions, respectively.

Table 14. Pitch rotation results of hydrodynamic analysis of sloshing effect of an FLNG vessel. Note: The number 0 represents a negligible response between considering (or not) the internal fluid dynamics. The number 1 indicates the highest response between considering (or not) the internal fluid dynamics.

Pitch Rotation																
Filling Fraction	Prismatic Tank				Divided Prismatic Tank				Spherical Tank				Cylindrical Tank			
	OP		H		OP		H		OP		H		OP		H	
	D	ND	D	ND	D	ND	D	ND	D	ND	D	ND	D	ND	D	ND
10%	1	0	0	1	0	1	0	1	0	1	0	1	0	0	0	0
20%	0	1	0	1	0	1	0	1	0	1	0	1	0	1	0	1
30%	0	1	0	1	1	0	1	0	1	0	1	0	1	0	1	0
40%	0	1	0	1	1	0	1	0	1	0	1	0	1	0	1	0
50%	0	1	0	1	0	1	1	0	0	1	0	1	1	0	1	0
60%	0	1	0	1	1	0	0	1	0	1	0	1	0	1	0	1
70%	0	1	0	1	0	1	0	1	1	0	0	1	1	0	1	0
80%	0	1	0	1	1	0	1	0	0	1	0	1	1	0	1	0

4. Conclusions

A methodology was developed to predict the sloshing effect on the global response of an FLNG vessel with four geometrical arrangements of storage tanks. The methodology considered the hydrodynamic analysis of the FLNG vessel employing environmental data from the Gulf of Mexico based on a return time of 10 years for a calm sea and 100 years for a stormy sea. FEM models and rules of DNV-GL society were used to estimate the sloshing effect behavior regarding regular operating (calm sea) and storm (hurricane) cases. In addition, the responses of the hydrodynamic analysis with and without considering the internal fluid dynamic in storage tanks of the FLNG vessel were compared. The maximum values of the sloshing effect were achieved for the divided prismatic tank for heave and roll accelerations and motions for regular operating and storm conditions. For pitch accelerations, the maximum value of the sloshing effect was shown for the spherical tank for regular operating conditions and the cylindrical tank for storm conditions. For pitch motions, the maximum value of these effects was obtained for the cylindrical tank considering regular operating and storm conditions.

Our results showed the importance of internal fluid dynamics in cargo tanks. The maximum responses calculated from the response spectrum were higher when internal fluid dynamics were included. Furthermore, the tank geometry and the filling fraction had an important impact on the behavior of the sloshing phenomenon. When fluid volume in tanks was smaller, the sloshing effects were higher.

Author Contributions: Methodology and software, D.F.H.-M.; investigation, results review discussion and writing review, I.F.-G.; supervision, J.H.-H.; writing-original draft preparation, D.F.H.-M.; writing-review and editing, A.L.H.-M. All authors have read and agreed to the published version of the manuscript.

Funding: The article processing charge (APC) was funded by Universidad Veracruzana.

Institutional Review Board Statement: Not applicable for studies not involving humans or animals.

Informed Consent Statement: Not applicable.

Data Availability Statement: Data are contained within the article.

Acknowledgments: Diego F. Hernández-Ménez thanks to Universidad Veracruzana and Instituto Mexicano del Petróleo.

Conflicts of Interest: The authors declare no conflict of interest.

References

1. Hu, Z.-Q.; Wang, S.-Y.; Chen, G.; Chai, S.-H.; Jin, Y.-T. The effects of LNG-tank sloshing on the global motions of FLNG system. *Int. J. Nav. Archit. Ocean. Eng.* **2017**, *9*, 114–125. [CrossRef]
2. Hernández-Ménez, D.F. Structural Analysis of Main Deck of an FPSO Vessel Supporting and Offshore Crane (Translation of Spanish). Master's Thesis, Universidad Veracruzana, Xalapa, Mexico, January 2020. Available online: https://www.uv.mx/veracruz/miaplicada/files/2021/07/Tesis_Diego-Hernandez-Menez.pdf (accessed on 17 May 2023).
3. Hernández-Ménez, D.F. Sloshing Effect Analysis of Global Response of an FLNG Vessel with Different Geometric Configurations of Tanks (Translation of Spanish). Bachelor's Thesis, Universidad Veracruzana, Xalapa, Mexico, December 2021.
4. Kim, S.-Y.; Kim, Y.; Ahn, Y.-J. Outlier analysis of sloshing impact loads on liquid ship cargo. *Proc. Inst. Mech. Eng. M J. Eng. Marit. Environ.* **2022**, *236*, 630–643. [CrossRef]
5. Lyu, W.; Riesner, M.; Peters, A.; Moctar, O.E. A hybrid method for ship response coupled with sloshing in partially filled tanks. *Marine Struct.* **2019**, *67*, 102643. [CrossRef]
6. Lee, S.J. The Effects of LNG-Sloshing on the Global Responses of LNG-Carriers. Ph.D. Thesis, Texas A&M University, College Station, TX, USA, May 2008. Available online: https://hdl.handle.net/1969.1/85945 (accessed on 20 May 2023).
7. Hosain, M.L.; Sand, U.; Fdhila, R.B. Numerical investigation of liquid sloshing in carrier ship fuel tanks. *IFAC-PpersOnLine* **2018**, *51*, 583–588. [CrossRef]
8. Ryu, M.C.; Jung, J.H.; Kim, Y.S.; Kim, Y. Sloshing design load prediction of a membrane type LNG cargo containment system with two-row tank arrangement in offshore applications. *Int. J. Nav. Archit. Ocean Eng.* **2016**, *8*, 537–553. [CrossRef]
9. Zheng, J.-H.; Xue, M.-A.; Dou, P.; He, Y.-M. A review on liquid sloshing hydrodynamics. *J. Hydrodyn.* **2021**, *33*, 1089–1104. [CrossRef]
10. Zheng, M.; Ni, Y.; Wu, C.; Jo, H. Experimental investigation on effect of sloshing on ship added resistance in head waves. *Ocean Eng.* **2021**, *235*, 109362. [CrossRef]
11. Wang, T.; Jin, H.; Lou, M.; Wang, X.; Liu, Y. Motion Responses of a Berthed Tank under Resonance Coupling Effect of Internal Sloshing and Gap Flow. *Water* **2021**, *13*, 3625. [CrossRef]
12. Zhu, Z.; Lee, J.; Kim, Y.; Lee, J.-H.; Park, T.-H. Experimental measurement and numerical validation of sloshing effects on resistance increase in head waves. *Ocean Eng.* **2021**, *234*, 109321. [CrossRef]
13. Zhuang, Y.; Wan, D. Numerical study on ship motion fully coupled with LNG tank sloshing in CFD method. *Int. J. Comput. Methods* **2018**, *15*, 18440022. [CrossRef]
14. DNV-GL. Available online: https://rules.dnv.com/docs/pdf/DNV/CG/2021-08/DNV-CG-0136.pdf (accessed on 2 February 2022).
15. DNV-GL. Available online: https://rules.dnv.com/docs/pdf/DNV/CG/2016-02/DNVGL-CG-0158.pdf (accessed on 2 February 2022).
16. Bureau Veritas. Available online: https://erules.veristar.com/dy/data/bv/pdf/554-NI_2011-05.pdf (accessed on 2 February 2022).
17. Dioni, P. Analysis of Wave Resonant Effects in-between Offshore Vessels Arranged Side-by-Side. Ph.D. Thesis, Universidad Politecnica de Madrid, Madrid, Spain, July 2016.
18. Dumitrache, C.L.; Deleanu, D. Sloshing effect, fluid structure interaction analysis. *IOP Conf. Ser. Mater. Sci. Eng.* **2020**, *916*, 012030. [CrossRef]
19. Xiangbo, L. Numerical Study of Liquid Sloshing in LNG Tanks Coupled with Ship Motions. Ph.D. Thesis, National University of Singapore, Singapore, 2015.
20. Krata, P.; Wawrzynski, W. Ship's rolling amplitude as a significant factor influencing liquid sloshing in partly filled tanks. *J. KONBiN* **2013**, *21*, 63–76. [CrossRef]
21. He, T.; Feng, D.; Liu, L.; Wang, X.; Jiang, H. CFD Simulation and Experimental Study on Coupled Motion Response of Ship with Tank in Beam Waves. *J. Mar. Sci. Eng.* **2022**, *10*, 113. [CrossRef]
22. Kawahashi, T.; Arai, M.; Wang, X.; Cheng, L.-Y.; Nishimoto, K.; Nakashima, A. A study on the coupling effect between sloshing and motion of FLNG with partially filled tanks. *J. Mar. Sci. Technol.* **2019**, *24*, 917–929. [CrossRef]
23. Lyu, W.; Moctar, O.e.; Schellin, E.T. Ship motion-sloshing interaction using a field method. *Marine Struct.* **2021**, *76*, 102923. [CrossRef]
24. DNV-GL. Available online: https://rules.dnv.com/docs/pdf/DNV/CG/2018-01/DNVGL-CG-0130.pdf (accessed on 2 February 2023).
25. Det Norske Veritas. SESAM User Manual Wadam Wave Analysis by Diffraction and Morrison Theory. Version 9.3. 2017. Available online: https://home.hvl.no/ansatte/tct/FTP/H2022%20Marinteknisk%20Analyse/SESAM/SESAM%20UM%20Brukermanualer/Wadam_UM.pdf (accessed on 26 May 2023).